ChemComm

COMMUNICATION

View Article Online
View Journal | View Issue

Cite this: *Chem. Commun.*, 2024, 60, 9444

Received 12th June 2024,
Accepted 1st August 2024

DOI: 10.1039/d4cc02851a

rsc.li/chemcomm

Electronic redistribution induced by interaction between ruthenium nanoparticles and Ni–N(O)–C sites boosts alkaline water electrolysis†

Jiacheng Wang, *[ab] Wangtao He,[b] Yuyang Zong,[c] Yanfeng Tang, [d] Jin Wang[d] and Ruguang Ma*[c]

Ultrafine ruthenium nanoparticles are encapsulated by single-atom Ni-bonded graphitic carbon nitride (g-C_3N_4) layers anchored on carbon nanotubes (Ru/Ni-CNCT). The enhanced electronic interaction between Ru nanoparticles and Ni–N(O)–C sites anchored in g-C_3N_4 layers promotes water adsorption/dissociation and hydrogen evolution.

With rapid industrialization and population growth, the energy crisis and environmental pollution have become global concerns. To alleviate these issues and achieve carbon neutrality, much attention has been paid to clean and sustainable energy sources.[1–3] As a clean energy carrier, hydrogen has three times the energy density (142 MJ kg^{-1}) of gasoline (47.3 MJ kg^{-1}) or diesel (44.8 MJ kg^{-1}), and is an ideal alternative to fossil fuels.[4,5] Electrocatalytic water splitting is a sustainable approach to producing high-purity hydrogen *via* a hydrogen evolution reaction (HER) at the cathode, concomitant with an oxygen evolution reaction (OER) at the anode. The harsh acidic environment and sluggish OER kinetics essentially limit the practical application of an acidic electrolyser.[6] Alternatively, alkaline water splitting has received much attention, due to the high activity and long-term stability of transition metal (TM)-based electrocatalysts toward OER.[7,8] To couple with alkaline OER for water electrolysis, cost-effective and efficient HER electrocatalysts are in high demand.

In an alkaline solution, an additional step of water dissociation to form adsorbed hydrogen makes the HER kinetics about 2–3 orders of magnitude slower than that in acidic media.[9,10] To solve this problem, Markovic's group carefully developed a strategy by depositing $Ni(OH)_2$ clusters on platinum electrode surfaces, where the edges of $Ni(OH)_2$ promote the dissociation of water. Then, the resultant hydrogen intermediates adsorb on nearby Pt sites and recombine into molecular hydrogen.[11] Inspired by this seminal work, many nanocomposites have been reported to synergistically promote water dissociation and hydrogen recombination.[12–14]

Ru as a Pt-group metal, shows better corrosion resistance and stability than Pt in alkaline conditions,[15–17] and is a promising alternative for the practical application of water splitting in alkaline media. However, in addition to water dissociation, the strong adsorption energy of H on Ru is another adverse factor to limit its catalytic activity, due to the unfavourable desorption of H on the Ru surface.[18] Modulating the desorption of H on Ru has been proven to be effective for improving HER performance. Qiao's group found that the adsorption energy of H can also be tailored by changing the Ru crystalline phase.[19] Face-centered cubic Ru_{fcc} has a lower d-band centre than that of hexagonal close packed Ru_{hcp}. Thus, the ΔG_H of Ru_{fcc} is more inclined to zero than that of Ru_{hcp}. Despite the remarkable achievements, it remains challenging to simultaneously regulate the water dissociation and adsorption of H at the active sites.

Herein, we report a nanocomposite electrocatalyst consisting of Ru nanoparticles encapsulated by graphitic carbon nitride (g-C_3N_4) with single-atom Ni–N(O)–C sites on carbon nanotubes (Ru/Ni-CNCTs) to simultaneously ameliorate water dissociation and H adsorption. By introducing carbon nanotubes as supports, electron transport during the HER process is greatly enhanced, which is beneficial for concerted electron–proton transfer. The intimate interface between the Ru surface and Ni–N(O)–C promotes electron transfer from the Ni atom to the Ru atom and lowers the adsorption energy of H, while Ni–N(O)–C boosts the nucleophilic attack of water at Ni sites and weakens the H–OH bond. The optimal Ru/Ni-CNCTs show high electrocatalytic activity with an overpotential of 35.4 mV at 10 mA cm^{-2} and a Tafel slope of 42 mV dec^{-1}, remarkably superior to the counterpart without Ni–N(O)–C sites.

[a] *Zhejiang Key Laboratory for Island Green Energy and New Materials, Institute of Electrochemistry, School of Materials Science and Engineering, Taizhou University, Taizhou 318000, Zhejiang, China. E-mail: jiacheng.wang@tzc.edu.cn*

[b] *State Key Laboratory of High-Performance Ceramics and Superfine Microstructure, Shanghai Institute of Ceramics, Chinese Academy of Sciences, Shanghai 200050, China*

[c] *School of Materials Science and Engineering, Suzhou University of Science and Technology, 99 Xuefu Road, Suzhou 215011, China. E-mail: ruguangma@usts.edu.cn*

[d] *College of Chemistry and Chemical Engineering, Nantong University, Nantong 226019, China*

† Electronic supplementary information (ESI) available. See DOI: https://doi.org/10.1039/d4cc02851a

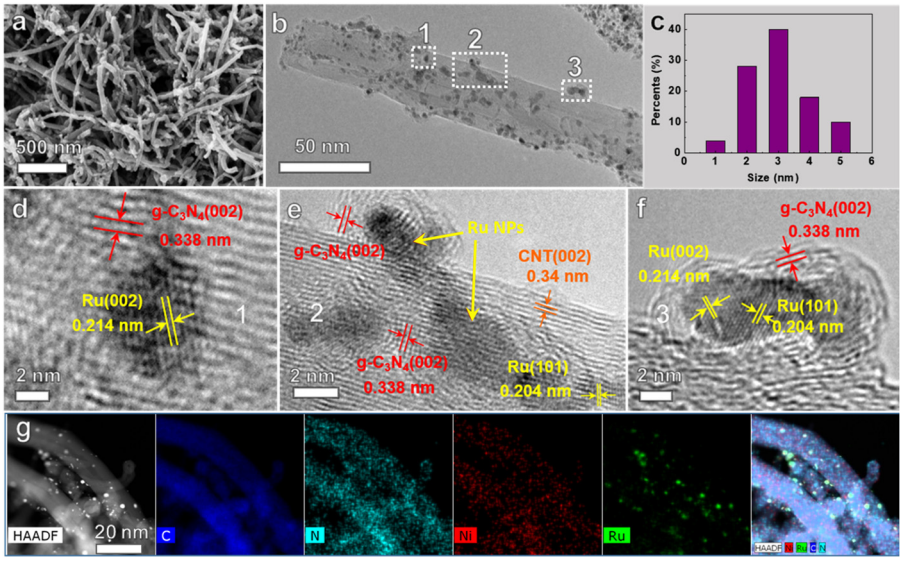

Fig. 1 (a) SEM image, (b) TEM image, (c) distribution of particle size of Ru nanoparticles anchored on Ni-CNCT. (d)–(f) HRTEM images of areas marked by dotted squares 1, 2 and 3 in (b), respectively. (g) HAADF-STEM image and elemental mappings of Ru/Ni-CNCT, implying the formation of Ru nanoparticles encapsulated by Ni single-atoms coordinated with g-C_3N_4 on carbon nanotubes.

Ru/Ni-CNCTs electrocatalysts were synthesized by a two-step method (Fig. S1, ESI†). Typically, a dicyanamide, Ni^{2+} source and carbon nanotubes were mixed homogenously and heated at 600 °C for 2 h in an Ar atmosphere to obtain g-C_3N_4 layers with rich Ni–N(O)–C sites on carbon nanotubes (Ni-CNCTs). After washing and drying, the powder was mixed with a certain amount of $RuCl_3 \cdot xH_2O$ and heated at 500 °C for 2 h. The final Ru/Ni-CNCTs were harvested after washing several times and drying overnight. Scanning electron microscopy (SEM) images show that Ru/Ni-CNCTs consist of many nanotubes decorated by bright metallic nanoparticles (Fig. 1a and Fig. S2, ESI†), while the SEM image of Ni-CNCTs shows no bright nanoparticles (Fig. S2a, ESI†). These bright nanoparticles are confirmed to be Ru nanoparticles by the enlarged SEM image and back-scattering electron images (Fig. S2b and c, ESI†). XRD patterns (Fig. S3a, ESI†) also show the presence of Ru peaks, compared to Ni/CNCT and pure carbon nanotubes. The Raman spectrum of Ru/Ni-CNCT (Fig. S3b, ESI†) reveals the fusion of g-C_3N_4 and carbon nanotubes. These results imply that the Ni atoms could bond with N atoms in g-C_3N_4, resulting in electron redistribution.[20] The transmission electron microscopy (TEM) image of Ru/Ni-CNCTs (Fig. 1b) shows many nanoparticles with sizes from 1 to 5 nm (Fig. 1c) anchored on carbon nanotubes with a diameter of ~20 nm. High-resolution TEM (HRTEM) images (Fig. 1d–f), corresponding to the areas marked by numbers 1–3, clearly reveal the details of the microstructure. In Fig. 1d, a nanoparticle with a size of 4 nm remarkably locates at the surface of the carbon nanotubes and the lattice fringes with spacings of 0.338 and 0.340 nm are indexed to plane (002) of Ru and (002) of carbon nanotubes, respectively. Fig. 1e clearly shows that the nanoparticles are encapsulated by few-layer g-C_3N_4, where the nanoparticles are assigned to Ru metal according to the lattice spacings and the outside layers are g-C_3N_4 coordinated with Ni single-atoms. A closer inspection (Fig. 1f) further confirms the unique microstructure, *i.e.*, Ru nanoparticle encapsulated by few-layer g-C_3N_4 coordinated with Ni single-atoms. Twin Ru nanoparticles with lattice spacings of 0.204 and 0.214 nm corresponding to (101) and (002), respectively, are wrapped by the g-C_3N_4 layers with a lattice spacing of 0.338 nm assigned to (002). In Fig. 1g, high-angle annular dark-field scanning TEM (HAADF-STEM) image and elemental mapping images show that C, N, and Ni signals are homogeneously distributed throughout Ru/Ni-CNCTs, while Ru signals show enrichment corresponding to Ru nanoparticles.

X-Ray absorption near-edge structure (XANES) spectra of the Ni K-edge in Fig. 2a show that the absorption threshold position in Ru/Ni-CNCT locates between Ni foil and NiO, and is much closer to that of NiO. This indicates that the valence of Ni in Ru/Ni-CNCT is approximately +2, suggesting the single-atom Ni sites possess a porphyrinic planar structure.[21] Furthermore, extended X-ray absorption fine structure (EXAFS) spectra show that Ru/Ni-CNCT exhibits one main peak at 1.54 Å, a little lower than that of the Ni–O peak (1.62 Å) in the spectrum of NiO, suggesting the existence of an Ni–N/O first coordination shell (Fig. 2b).[22] Compared to the Ni–Ni peak of Ni foil (2.19 Å), a weak Ni–Ni peak is also observed at 2.16 Å in the spectrum of Ru/Ni-CNCT, which should arise from a certain amount of Ni clusters. Based on this information, a postulated model of Ni–N(O)–C coordination was utilized to fit the EXAFS spectrum (inset of Fig. 2a). The fitting results indicate that the first shell of the Ni atom has a coordination number of 4.1 ± 1.2, corresponding to Ni–N/O (Fig. S4 and Table S1, ESI†). The wavelet transform (WT) contour plots are correspondingly assigned to Ni–N/O and Ni–Ni coordination (Fig. 2c).

X-Ray photoelectron spectroscopy (XPS) reveals the chemical states of the Ru/Ni-CNCT surface. Compared to two obvious peaks assigned to pyrrolic N (399.6 eV) and graphitic N (401.4 eV) of Ni-CNCT, the N 1s spectrum of Ru/Ni-CNCT changes remarkably (Fig. 2d). In particular, a new peak at 398.4 eV is present,

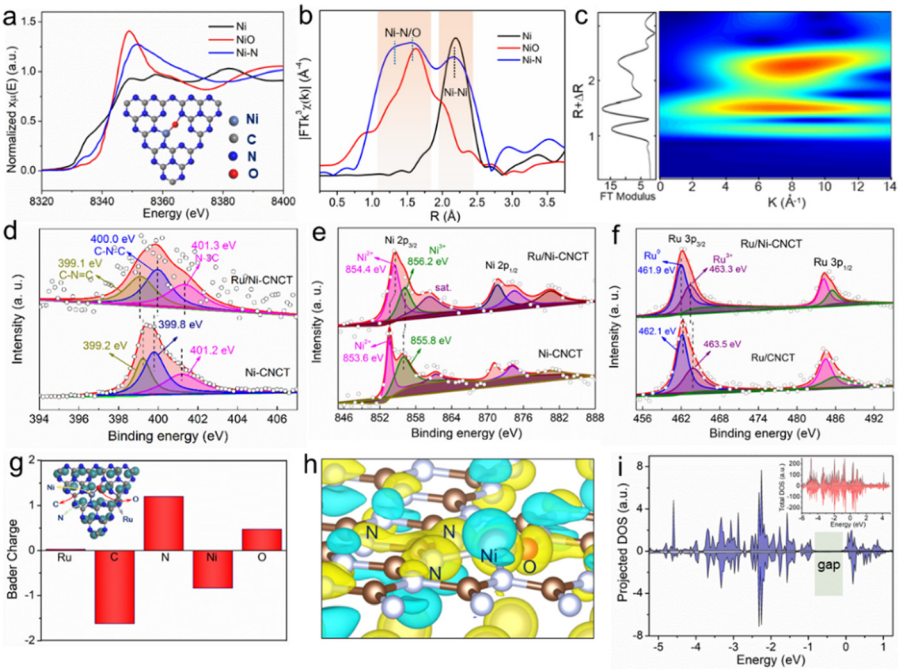

Fig. 2 (a) XANES (inset: proposed structure of Ni–N(O)–C coordination sites) and (b) FT-EXAFS of Ni K-edge spectra, (c) WT-EXAFS of the Ni K-edge of Ru/Ni-CNCT. High-resolution XPS spectra of (d) N 1s, (e) Ni 2p and (f) Ru 3p of Ru/Ni-CNCT. (g) Bader charge of Ru, C, N, Ni and O, (h) differential charge density in Ru/Ni–N(O)–C model (cyan and yellow represent the depletion and accumulation of electrons, respectively) and (i) pDOS of Ni and total DOS of Ru/Ni–N(O)–C.

due to the presence of pyridinic N or N–Ni. Additionally, a peak at 403.4 eV assigned to N oxide also appears. These two additional peaks are very consistent with the XANES and EXAFS results. The high-resolution Ni 2p XPS results indicate that two peaks at 854.7 and 871.8 eV can be assigned to Ni $2p_{3/2}$ and Ni $2p_{1/2}$, respectively, and two corresponding satellite peaks locate at 860.4 and 880.6 eV. Compared to Ni-CNCT, the relative content of the Ni^{2+} component in Ru/Ni-CNCT increases, indicating that the dominant valence is close to +2,[23] which is consistent with the XANES results.

Moreover, the binding energy of Ni 2p in Ru/Ni-CNCT shifts positively compared to that in Ni-CNCT, demonstrating electron loss by Ni. XPS spectra of Ru 3p show two peaks located at 462.1 and 484.4 eV, corresponding to Ru $3p_{1/2}$ and Ru $3p_{3/2}$, respectively, which can be deconvoluted into dominant Ru^0 and partial Ru^{3+}. Compared to Ru/CNCT, the binding energy of Ru 3p peaks shifts slightly in the low binding energy direction, indicating electron gain possibly from Ni sites. To further confirm such electron transfer, density functional theory (DFT) calculations were conducted by building a structural model (Fig. S5, ESI†) based on the HRTEM observation. As shown in Fig. 2g, the Bader charges of Ru, N and O are +0.008, +1.206, +0.477 in order, suggesting electron gain, while the Bader charges of Ni and C are −0.838 and −1.617, respectively, indicating electron loss. The differential charge density illustrates strong charge redistribution among these atoms when the g-C_3N_4 layer with Ni–N(O)–C sites encapsulates Ru nanoparticles (Fig. 2h), where an obvious electron-deficient distribution (light blue area) locates at the Ni atom and electron-rich distribution (yellow area) at the N and O atoms. The obvious gap around the Fermi level in the projected density of states (pDOS) of Ni also indicates the electron loss of Ni atoms (Fig. 2i), whereas the total DOS retains a conductive characteristic (inset of Fig. 2i). The strong electron redistribution of Ni–N(O)–C coordination with Ru nanoparticles is expected to promote water adsorption/adsorption and subsequent hydrogen desorption.[24]

Linear scanning voltammetry (LSV) curves (Fig. 3a) show that Ru/Ni-CNCT exhibits much higher activity than Ni-CNCT or Ru/CNCT, and approaches the activity of commercial Pt/C in terms of onset potential and overpotential at 10 mA cm^{-2}. Ru/Ni-CNCT shows an overpotential of 35.4 mV at 10 mA cm^{-2} and 97.6 mV at 50 mA cm^{-2}, respectively, much smaller than that of Ru/CNCT (70.7 and 221.9 mV) and close to that of Pt/C (28.0 and 79.0 mV). In contrast, Ni-CNCT shows no obvious activity toward HER. The Tafel slope of Ru/Ni-CNCNT is 42 mV dec^{-1} (Fig. 3b), much lower than that of Ru/CNCT (63 mV dec^{-1}), suggesting that the HER follows the Volmer–Heyrovsky mechanism. It also implies that the electron redistribution induced by the Ni–N(O)–C sites enhances water dissociation kinetics and improves the whole HER process. In addition, based on the Tafel slope, the exchange current density of Ru/Ni-CNCT is calculated to be about 0.79 mA cm^{-2}, much higher than the 0.60 mA cm^{-2} of Ru/CNCT, indicating obviously improved reaction kinetics. These results undoubtedly indicate that the sluggish Volmer step is accelerated by the electronic interaction between Ru atoms and Ni-CNCT, as illustrated in Fig. 2f–g. A series of samples were also synthesized to obtain the optimal sample by changing the content of Ru or Ni during the synthesis process. When the content of Ru is 5 wt% and the content of Ni is 1.0 wt%, the as-prepared Ru/Ni-CNCT exhibits the best electrocatalytic performance (Fig. S6–S8, ESI†). Moreover, this strategy can be extended to other single-atom TM–N(O)–C sites, such as Ru/Fe-CNCT and Ru/Co-CNCT (Fig. S9, ESI†). Among them, Ru/Ni-CNCT still shows the best electrocatalytic activity, which is close to that of commercial Pt/C.

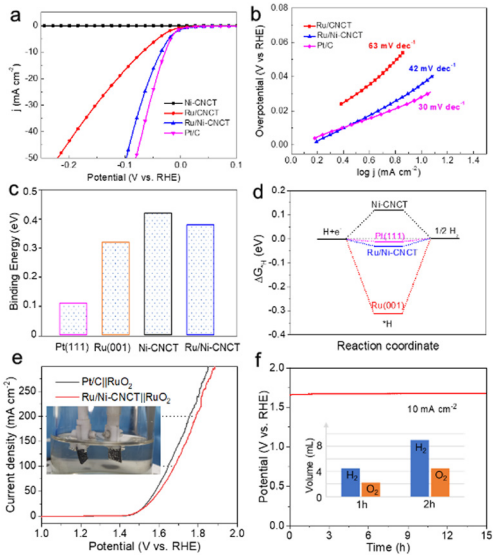

Fig. 3 (a) LSV curves and (b) corresponding Tafel slopes of Ni-CNCT, Ru/CNCT, Ru/Ni-CNCT and Pt/C. (c) Binding energy of water molecules (ΔE_w) and (d) Gibbs free energy of H adsorption (ΔG_{*H}) at the surface of Pt (111), Ru (001), Ni–N(O)–C and Ru/Ni–N(O)–C, corresponding to Pt/C, Ru/CNCT, Ni-CNCT and Ru/Ni-CNCT, respectively. (e) LSV curves of Pt/C||RuO_2 and Ru/Ni-CNCT||RuO_2, respectively, and (f) long-term stability of Ru/Ni-CNCT||RuO_2 and the corresponding volume of H_2 and O_2 after 1 hour and 2 hours.

To understand the underlying reasons, the binding energy of an H_2O molecule (ΔE_w) and Gibbs free energy of hydrogen adsorption (ΔG_{*H}) were calculated by DFT. To get the ΔE_w of Pt/C and Ru/CNCT, highly active Pt (111) and Ru (001) are used as the adsorption surfaces, respectively. Ru/Ni-NCNT shows a higher binding energy (0.38 eV) than Pt (111) or Ru (001), indicating good capability for water dissociation (Fig. 3c). Ni-CNCT shows the highest ΔE_w due to the N-rich structural surface, but Ni-CNCT also shows a more positive ΔG_{*H}. This implies that Ni-CNCT with unique single-atom Ni–N(O)–C sites has good ability to dissociate a water molecule but very poor adsorption energy for a proton. This would cause poisoning of the active surface by the *OH produced from water dissociation. Ru/Ni-NCNT not only shows strong water-dissociation ability, but also exhibits a moderate ΔG_{*H} (−0.03 eV), as shown in Fig. 3d, very close to that of Pt (111) (−0.01 eV). These two key factors remarkably boost the reaction kinetics of HER in an alkaline solution.

To demonstrate the application potential for water electrolysis, an alkaline electrolytic cell was assembled by using the optimal Ru/Ni-CNCT as the HER electrocatalyst and commercial RuO_2 as the OER electrocatalyst (inset of Fig. 3e). The LSV curve of Ru/Ni-CNCT||RuO_2 shows a little larger overpotential (31 mV at 100 mA cm^{-2} and 34 mV at 200 mA cm^{-2}) compared to that of Pt/C||RuO_2 (Fig. 3e). The stability measurement of Ru/Ni-CNCT||RuO_2 shows that the voltage remains almost stable, and increases only 0.9% over 15 h. The produced H_2 and O_2 were also collected with home-made equipment (Fig. S10, ESI†). The volumes of H_2 and O_2 are about 9.0 and 4.5 mL after two hours, respectively (Fig. 3f), consistent with the theoretical ratio of 2 : 1 and close to the theoretical values of 9.14 and 4.57 mL, which indicates that the Faraday efficiency of water splitting is almost 100%.

In summary, Ru nanoparticles encapsulated by g-C_3N_4 layers with single-atom Ni–N(O)–C sites on carbon nanotubes have been successfully synthesized by a facile two-step method. The reaction kinetics of critical HER steps in alkaline solution is accelerated by the electronic interaction between Ru nanoparticles and Ni-bonded g-C_3N_4. This work provides a new strategy to design cost-effective electrocatalysts toward hydrogen production by water splitting.

This work is financially supported by National Natural Science Foundation of China (52172058, 92163117, 52072389), the Science and Technology Commission of Shanghai Municipality (22DZ1205600). We are grateful to the Shanghai Synchrotron Radiation Facility (SSRF) for the Beamtime for the XAFS measurements.

Data availability

Data available within the article or its ESI.†

Conflicts of interest

There are no conflicts to declare.

Notes and references

1 M. Chatenet, B. G. Pollet, D. R. Dekel, F. Dionigi, J. Deseure, P. Millet, R. D. Braatz, M. Z. Bazant, M. Eikerling, I. Staffell, P. Balcombe, Y. Shao-Horn and H. Schäfer, *Chem. Soc. Rev.*, 2022, **51**, 4583–4762.
2 G. Martí, L. Mallón, N. Romero, L. Francàs, R. Bofill, K. Philippot, J. García-Antón and X. Sala, *Adv. Energy Mater.*, 2023, **13**(21), 2300282.
3 H. Zhu, J. J. Wang, Z. Xu and Y. Tan, *Small*, 2024, **20**, 2404919.
4 M. Lao, P. Li, Y. Jiang, H. Pan, S. X. Dou and W. Sun, *Nano Energy*, 2022, **98**, 107231.
5 Q. Yang, X. Tong and Z. Wang, *Mater. Rep. Energy*, 2024, **4**, 100253.
6 G. Qian, J. Chen, T. Yu, J. Liu, L. Luo and S. Yin, *Nano-Micro Lett.*, 2021, **14**, 20.
7 Z. Li, X. Wu, X. Jiang, B. Shen, Z. Teng, D. Sun, G. Fu and Y. Tang, *Adv. Powder Mater.*, 2021, **1**(2), 100020.
8 Y. Feng, N. Ran, X. Wang, Q. Liu, J. Wang, L. Liu, K. Suenaga, W. Zhong, R. Ma and J. Liu, *Adv. Energy Mater.*, 2023, **13**, 2302452.
9 B. Sang, C. Xue, S. Guo, X. Wng, S. Xie, C. Wang and R. Q. Li, *Chem. Commun.*, 2024, **60**, 6643–6646.
10 X. W. Lv, W. W. Tian and Z. Y. Yuan, *Electrochem. Energy Rev.*, 2023, **6**, 23.
11 R. Subbaraman, D. Tripkovic, D. Strmcnik, K.-C. Chang, M. Uchimura, A. P. Paulikas, V. Stamenkovic and N. M. Markovic, *Science*, 2011, **334**, 1256–1260.
12 D. Wu, D. Chen, J. Zhu and S. Mu, *Small*, 2021, **17**, 2102777.
13 B. Wang, J. Li, D. Li, J. Xu, S. Liu, Q. Jiang, Y. Zhang, Z. Duan and F. Zhang, *Adv. Mater.*, 2024, **36**, 2305437.
14 Q. Hu, K. Gao, X. Wang, H. Zheng, J. Cao, L. Mi, Q. Huo, H. Yang, J. Liu and C. He, *Nat. Commun.*, 2022, **13**, 3958.
15 Y. Zhang and Q. Yuan, *Chem. Commun.*, 2024, **60**, 7188–7191.
16 J. Creus, S. Drouet, S. Suriñach, P. Lecante, V. Collière, R. Poteau, K. Philippot, J. García-Antón and X. Sala, *ACS Catal.*, 2018, **8**(12), 11094–11102.
17 P. Xue, M. Qiao, J. Miao, Y. Tang, D. Zhu and C. Guo, *Chem. Commun.*, 2024, **60**, 6423–6426.
18 Y. Yang, Y. Yu, J. Li, Q. Chen, Y. Du, P. Rao, R. Li, C. Jia, Z. Kang, P. Deng, Y. Shen and X. Tian, *Nano-Micro Lett.*, 2021, **13**, 160.
19 Y. Zheng, Y. Jiao, Y. Zhu, L. H. Li, Y. Han, Y. Chen, M. Jaroniec and S. Z. Qiao, *J. Am. Chem. Soc.*, 2016, **138**, 16174–16181.
20 P. Rao, Y. Deng, W. Fan, J. Luo, P. Deng, J. Li, Y. Shen and X. Tian, *Nat. Commun.*, 2022, **13**, 5071.
21 W. Wan, Y. Zhao, S. Wei, C. A. Triana, J. Li, A. Arcifa, C. S. Allen, R. Cao and G. R. Patzke, *Nat. Commun.*, 2021, **12**, 5589.
22 S. Li, R. Ma, J. Hu, Z. Li, L. Liu, X. Wang, Y. Lu, G. E. Sterbinsky, S. Liu, L. Zheng, J. Liu, D. Liu and J. Wang, *Nat. Commun.*, 2022, **13**, 2916.
23 Y. Dang, T. Wu, H. Tan, J. Wang, C. Cui, P. Kerns, W. Zhao, L. Posada, L. Wen and S. L. Suib, *Energy Environ. Sci.*, 2021, **14**, 5433–5443.
24 Y. Feng, X. Wang, J. Ma, N. Wang, Q. Liu, K. Suenaga, W. Chen, J. Zhang, Y. Zhou and J. Wang, *Adv. Energy Mater.*, 2024, **14**, 202401501.